

Polar active liquids: a universal classification rooted in non-conservation of momentum

Khanh-Dang Nguyen Thu Lam, Michael Schindler, Olivier Dauchot

UMR Gulliver 7083 CNRS, ESPCI ParisTech, PSL Research University, 10 rue Vauquelin, 75005 Paris, France

Abstract. We study the spatially homogeneous phases of polar active particles in the low density limit, and specifically the transition from the isotropic phase to collective polar motion. We show that the fundamental quantity of interest for the stability of the isotropic phase is the forward component of the momentum change induced by binary scattering events. Building on the Boltzmann formalism, we introduce an ansatz for the one-particle distribution and derive a closed-form evolution equation for the order parameter. This approach yields a very intuitive and physically meaningful criterion for the destabilization of the isotropic phase, where the ansatz is exact. The criterion also predicts whether the transition is continuous or discontinuous, as illustrated in three different classes of models. The theoretical predictions are in excellent agreement with numerical results.

1. Introduction

Polar active liquids are composed of aligning self-propelled particles which convert energy into directed motion. They generically exhibit large scale collective motion [1, 2]. Simulations of Vicsek-like models of constant-speed point particles, aligning with their neighbors in the presence of noise, have revealed the existence of a transition between an isotropic phase and a true long-range order polar phase with giant density fluctuations [3, 4, 5, 6, 7, 8]. For metric interactions—with a density-dependent rate of collisions—the homogenous polar state is unstable close to the transition; propagative structures develop and the transition becomes discontinuous. An intense theoretical effort towards the understanding of the long range behavior of these systems has lead to the picture of a basic universality class, at least for the simplest situation in which the surrounding fluid can be neglected (dry flocking) and the sole interaction is some local alignment [9, 10, 11, 12, 13, 14, 15, 16, 17, 18, 19].

However, Vicsek-like models contain some level of coarse-graining of the dynamics and as such are not just “simple liquids” [20]. For a given system of particles, either be it experimental [21, 22, 23, 24, 25, 26, 27, 28] or numerical [29, 30, 31, 32, 33], it is thus crucial to check whether it indeed belongs to the above universality class. This question has been addressed in a very limited number of experimental situations only. In the case of rolling colloids [26], for which the hydrodynamics equations can be derived explicitly, the interactions mediated by the surrounding fluid actually dominate the alignment mechanism, but also screen the splay instability responsible for giant density fluctuations in the polar phase. In the case of walking grains [22, 25], the alignment mechanism results from complex re-collisional dynamics, and large-scale simulations reveal some qualitative differences with the above canonical scenario [34].

In some sense, both the complexity of the dynamics close to the transition, and the technicality of the derivation of the hydrodynamic equations have hindered a more basic question: is there a simple way to predict the existence and the order of a transition to collective motion for a given microscopic dynamics? In this Letter, we tackle this question, restricting ourselves to the study of the homogeneous phases of two-dimensional polar active liquids in the low density limit. In such systems, the total momentum is changed by binary scattering and self-diffusion events. We start from the Boltzmann equation formalism, assuming that the molecular chaos hypothesis holds. With no further assumptions, we first derive an evolution equation for the total momentum. However, this evolution equation depends on the unknown angular distribution of the particle velocities. We then propose an ansatz for this distribution, and obtain a closed-form equation for the order parameter. Applying this equation in the isotropic phase, where the ansatz is exact, we introduce a physically meaningful *effective alignment*, which simply is the average over all binary scattering events of the non-conserved part of the momentum, projected on the momentum before scattering. The transition to collective motion occurs when this effective alignment is larger than the disaligning effect of self-diffusion. A similar criterion also predicts whether the transition

is continuous or discontinuous. Finally, we test and illustrate our approach on (i) a mean-field Vicsek-like model (ii) a continuous-time model of hard disks obeying Vicsek aligning rules when colliding, actually an implementation of the BDG model [12, 13], and (iii) a model of self-propelled inelastic hard disks. In all cases not only the transition point is very well predicted, but the ansatz also works surprisingly well, even far in the polar phase.

In the light of the important role played by inhomogeneous solutions, focusing on the transition between homogeneous phases may look a bit academic. However, revisiting the transition towards collective motion in terms of phases and phase separations, has recently proven to be an insightful approach [35, 36, 37]. Furthermore, following the experimental discovery of topological interactions —with a density-independent rate of collision—in bird flocks [38], it was shown that such systems remain homogeneous across the transition [7, 15, 16, 39, 40]. Also, experimental systems of interest may have small enough sizes such that homogeneous phases are stable. Finally, we shall see that following this route leads us towards a very intuitive understanding of the conditions which particle interaction must satisfy to induce a transition towards collective motion.

2. Theoretical framework

Particle velocities at equilibrium obey the Maxwell-Boltzmann distribution; self-propelled particles do not. After some transient, a self-propelled particle reaches its intrinsic steady velocity v_0 , set by the competition between propelling and dissipation mechanisms [41, 42, 43]. In the low-density limit, this transient lasts much less than the mean free flight time, and one can safely assume that particles have a constant speed v_0 . For spatially homogeneous states, the one-particle distribution thus reduces to the density probability $f(\theta, t)$ of having a particle with velocity $v_0\hat{\mathbf{e}}(\theta)$ at time t , where $\hat{\mathbf{e}}(\theta)$ is the unit vector of polar angle θ . This distribution evolves according to self-diffusion events and binary scattering events. A binary scattering event begins when two particles start interacting and ends when they recover their speed v_0 ; it can be rather complex, involving for instance successive re-collisions, as in systems of hard disks [41]. For a binary scattering picture to be valid, the typical scattering time and length need to be of the order of the microscopic scales. Also, it requires the interactions to be binary, thus excluding in principle the case of long-range interactions, such as hydrodynamics interactions in active suspensions. In general, the scattering of two self-propelled particles does not conserve the average momentum of the system $\mathbf{P}(t) = \int d\theta f(\theta, t) \hat{\mathbf{e}}(\theta)$. Taking $\psi(t) = |\mathbf{P}(t)|$ as the order parameter of the transition towards polar collective motion, it is thus natural to analyze the change of momentum *at the level of binary scattering*. As we shall see, this allows to understand collective macroscopic states, starting from a microscopic description.

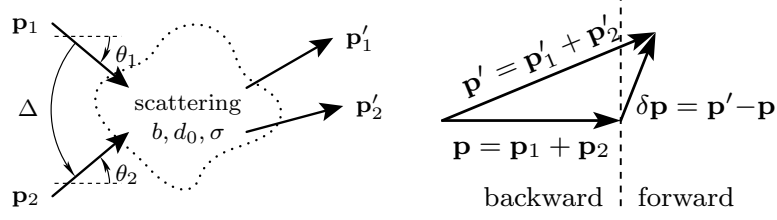


Figure 1. *Left:* Scattering of two particles. *Right:* Criterion for stability of the isotropic phase. The momentum of two interacting particles is changed from \mathbf{p} to \mathbf{p}' . If \mathbf{p}' is more likely to be found in the forward semi-plane, the isotropic state is unstable.

2.1. Kinetic equations

Within our approximations, the evolution equation for $f(\theta, t)$ is given by the Boltzmann equation [13]:

$$\frac{\partial f}{\partial t}(\theta, t) = I_{\text{scat}}[f, f] + I_{\text{diff}}[f], \quad (1)$$

where the binary scattering contribution is given by the scattering integral $I_{\text{scat}}[f, f]$ and where the self-diffusion process is given by $I_{\text{diff}}[f]$. An integration of this equation over θ , using $\int d\theta \hat{\mathbf{e}}(\theta)$, leads to a kinetic equation for $\mathbf{P}(t)$. Here, we find it more instructive to obtain such a kinetic equation by using an equivalent but more elementary derivation.

A scattering event, as pictured schematically on Fig. 1(left), is specified by the incoming angles θ_1 and θ_2 of the two particles or, equivalently, by the incoming half-angle $\bar{\theta} = \text{Arg}(e^{i\theta_1} + e^{i\theta_2})$ and the incoming angular separation $\Delta = \theta_1 - \theta_2$. Additional scattering parameters, such as the impact parameter, or some collisional noise, may be needed and are collectively noted as ζ . A scattering event changes the momentum sum of the involved two particles by an amount $\delta\mathbf{p}$, which depends a priori on all scattering parameters $\bar{\theta}$, Δ and ζ . The average momentum of all N particles in the system changes in this event from \mathbf{P} into \mathbf{P}' , concluding that $N(\mathbf{P}' - \mathbf{P}) = \delta\mathbf{p}$. In the same way, a self-diffusion event changes the momentum of a particle at θ_1 by an amount $N(\mathbf{P}' - \mathbf{P}) = \delta\mathbf{p}_{\text{diff}}(\theta_1, \eta) = \mathbf{R}_\eta \mathbf{p} - \mathbf{p}$, where $\mathbf{R}_\eta \mathbf{p}$ is the rotation of $\mathbf{p} = \hat{\mathbf{e}}(\theta_1)$ by an angle η . The self-diffusion process is characterized by the probability density $P_\eta(\eta)$ for a particle with angle θ_1 to jump to angle $\theta_1 + \eta$. Assuming molecular chaos and averaging these two balance equations over the statistics of scattering and self-diffusion events taking place in a small time interval, one obtains the evolution equation by taking the continuous time limit:

$$\frac{d\mathbf{P}}{dt} = \lambda \Phi_f^{\text{scat}}[\delta\mathbf{p}(\bar{\theta}, \Delta, \zeta)] + \lambda_{\text{diff}} \Phi_f^{\text{diff}}[\delta\mathbf{p}_{\text{diff}}(\theta_1, \eta)], \quad (2)$$

where

$$\Phi_f^{\text{scat}}[\dots] = \int_0^{2\pi} d\bar{\theta} \int_{-\pi}^{\pi} d\Delta \int d\zeta K(\Delta, \zeta) f(\theta_1, t) f(\theta_2, t) (\dots), \quad (3)$$

$$\Phi_f^{\text{diff}}[\dots] = \int_0^{2\pi} d\theta_1 \int d\eta P_\eta(\eta) f(\theta_1, t) (\dots). \quad (4)$$

In the right hand side of Eq. (2), the second term comes from the self-diffusion process, which happens at a characteristic rate λ_{diff} . The first term comes from the binary scattering process. In its integrand, a scattering event with scattering parameters θ_1 , θ_2 and ζ is assumed to happen at a rate proportional to both $f(\theta_1, t)$ and $f(\theta_2, t)$; this comes from the molecular chaos hypothesis. The proportionality factor is $\lambda K(\Delta, \zeta)$, the scattering rate of such an event. Note that it does not depend on $\bar{\theta}$ as a result of global rotational invariance. As a convention, we have chosen to normalize K such that $\frac{1}{2\pi} \int_{-\pi}^{\pi} d\Delta \int d\zeta K(\Delta, \zeta) = 1$. The prefactor λ thus gives the characteristic scale of the scattering rate. In what follows, we shall consider two cases.

(i) Non-metric models: In a model without space, λ is a free parameter and $K(\Delta, \zeta) = K(\zeta)$ does not depend on Δ .

(ii) Metric models: If one considers interacting disks with diameter d_0 at a density number ρ , a scattering event is entirely described by θ_1 , θ_2 and the impact parameter b (thus, $\int d\zeta \equiv \int_{-d_0}^{d_0} db$). By using the construction of the Boltzmann cylinder [44], one finds for the scattering rate $\lambda K(\Delta, b) = \rho v_0 |\sin \frac{\Delta}{2}|$. Importantly, it is proportional to the density and does not depend on the impact parameter. The Boltzmann cylinder expresses the fact that tangential scattering (small $|\Delta|$) occurs at a smaller rate than frontal scattering (large $|\Delta|$). Indeed, in tangential scattering, particles are more parallel and, having the same speed, have a smaller relative velocity, hence a smaller scattering rate. On the other hand, particles have a higher relative velocity in frontal scattering, hence a larger scattering rate.

Equation (2) gives the evolution of the vectorial order parameter \mathbf{P} . Now, in order to get the evolution of $\psi = |\mathbf{P}|$, we go to polar coordinates $\mathbf{P} = \psi \hat{\mathbf{e}}(\theta_P)$ and project Eq. (2) on the radial direction $\hat{\mathbf{e}}(\theta_P)$. When the scattering and self-diffusion processes obey the mirror symmetry (no chirality), \mathbf{P} keeps its angular direction, so that one can set $\theta_P(t) = 0$. As for the binary scattering term, we find for the projection $\Phi_f^{\text{scat}}[\delta \mathbf{p}] \cdot \hat{\mathbf{e}}(\theta_P) = \Phi_f^{\text{scat}}[(\hat{\mathbf{p}} \cdot \delta \mathbf{p}) \cos \bar{\theta}]$. For the self-diffusion term, we can compute the integral explicitly and obtain $\lambda_{\text{diff}} \Phi_f^{\text{diff}}[\delta \mathbf{p}_{\text{diff}}] = -D\psi$, where the self-diffusion constant is given by

$$D = \lambda_{\text{diff}} \left(1 - \int d\eta P_\eta(\eta) \cos \eta \right) \geq 0. \quad (5)$$

It is instructive to look at an angular noise with zero expectation and variance σ_0^2 . Using $P_\eta(\eta) = \exp(-\eta^2/2\sigma_0^2)/\sqrt{2\pi\sigma_0^2}$, one finds $D = \lambda_{\text{diff}}(1 - e^{-\sigma_0^2/2})$. In particular, when the angular noise is weak, $\sigma_0 \ll 1$, one has $D \propto \sigma_0^2$.

Altogether, the radial component of Eq. (2) reads:

$$\frac{d\psi}{dt} = \lambda \Phi_f^{\text{scat}}[(\hat{\mathbf{p}} \cdot \delta \mathbf{p}) \cos \bar{\theta}] - D\psi. \quad (6)$$

This evolution equation is derived from Eq. (2) with the only additionnal assumption that the system is not chiral. We keep this assumption in what follows.

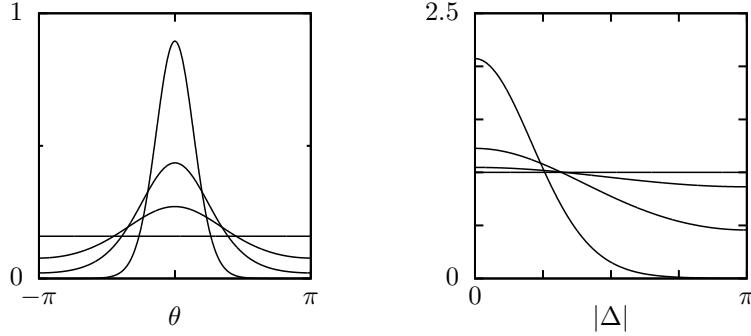


Figure 2. *Left:* the von Mises distribution $f_\psi(\theta)$, for $\psi = 0, 0.3, 0.6$ and 0.9 . *Right:* the kernel $g(\psi, \Delta)/\psi$ for the same values of ψ .

2.2. The von Mises distribution ansatz

The above kinetic equations remain of limited practical interest as long as the angular distribution f is unknown. Here, we propose an ansatz of the form $f(\theta, t) = f_{\psi(t)}(\theta)$, which we constrain to be exact in the isotropic phase. We choose f_ψ to be the so-called von Mises distribution [45], the distribution of random angles, uniform up to the constraint $|\int d\theta f_\psi(\theta) \hat{\mathbf{e}}(\theta)| = \psi$. This distribution maximizes the entropy functional $H[f] = -\int f \log f$ under the aforementioned constraint and is, in this sense, the simplest ansatz one can think of and was actually used to study Vicsek-like models [46, 47]. It is parameterized by the order parameter ψ in the following way:

$$f_\psi(\theta) = \frac{e^{\kappa(\psi) \cos \theta}}{2\pi I_0(\kappa(\psi))}, \quad \text{with} \quad \frac{I_1(\kappa)}{I_0(\kappa)} = \psi, \quad (7)$$

where $I_n(x)$ is the modified Bessel function of the first kind, of order n . Plots of this distribution for different values of ψ are available in Fig. 2 (left). In the limits $\psi \rightarrow 0$ ($\kappa \rightarrow 0$) and $\psi \rightarrow 1$ ($\kappa \rightarrow \infty$), one recovers respectively the isotropic distribution $f(\theta) = 1/2\pi$ and a normal distribution of variance $1/\kappa$. For all values of ψ (equivalently of κ), this distribution has a single maximum at $\theta = 0$ and a single minimum at $\theta = \pm\pi$. It is more peaked as ψ or κ is higher. The symmetry $\theta \leftrightarrow -\theta$ expresses the non-chirality of the system. After injecting this ansatz into Eq. (6), the integration over $\bar{\theta}$ can be performed analytically. Because the ansatz is parameterized by ψ , one obtains a closed-form equation for the evolution of ψ :

$$\frac{1}{\lambda} \frac{d\psi}{dt} = F(\psi) - \frac{D}{\lambda} \psi, \quad (8)$$

The binary scattering term $F(\psi)$ is a (non-linear) function of ψ and a functional of the scattering function $\mathbf{p} \cdot \delta\mathbf{p}(\Delta, \zeta)$:

$$F(\psi) = \int_{-\pi}^{\pi} \frac{d\Delta}{2\pi} \int d\zeta K(\Delta, \zeta) g(\psi, \Delta) \mathbf{p} \cdot \delta\mathbf{p}(\Delta, \zeta), \quad (9)$$

where

$$g(\psi, \Delta) = \frac{\kappa(\psi)}{I_0(\kappa(\psi))^2} \frac{I_1(2\kappa(\psi) \cos \frac{\Delta}{2})}{2\kappa(\psi) \cos \frac{\Delta}{2}}. \quad (10)$$

The kernel $g(\psi, \Delta)$ is plotted in Fig. 2 (right). Its behaviour can be interpreted in the following way. As the system is more polar (higher ψ), it is more likely to find pairs of aligned particles than anti-aligned particles: scattering at low values of $|\Delta|$ is favored as compared to scattering at $|\Delta| \simeq \pi$. Around the isotropic state $\psi \ll 1$, one has $g(\psi, \Delta) \simeq \psi$, which, as expected, does not depend on Δ . The accuracy of the ansatz, and hence the accuracy of g , are tested numerically below.

2.3. Instability of the isotropic state: a proper definition of the alignment

To account for the destabilization of the isotropic state, one must consider the spontaneous fluctuations of $\psi \ll 1$. At linear order in ψ , the von Mises distribution reads

$$f_\psi(\theta) = \frac{1}{2\pi}(1 + 2\psi \cos \theta). \quad (11)$$

Note that this distribution verifies the self-consistency condition $|\int d\theta f_\psi(\theta) \hat{\mathbf{e}}(\theta)| = \psi$. This is the distribution one would obtain, assuming that the orientations of the particles are not correlated, the most reasonable assumption for the isotropic phase. It is in this sense that the ansatz can be said to be exact for the description of the isotropic state. At linear order in ψ , Eq. (8) reads

$$\frac{1}{\lambda} \frac{d\psi}{dt} = \mu\psi, \quad (12)$$

where

$$\mu = \langle \mathbf{p} \cdot \delta \mathbf{p} \rangle_0 - \frac{D}{\lambda} \quad (13)$$

with

$$\langle \dots \rangle_0 = \int_{-\pi}^{\pi} \frac{d\Delta}{2\pi} \int d\zeta K(\Delta, \zeta) (\dots). \quad (14)$$

The above set of equations is our central result. It is exact within the approximations of the Boltzmann equation for non-chiral systems. As we shall see now, it provides an intuitive understanding of when polar collective motion develops in systems of polar active particles and allows to define properly the alignment of scattering events. The isotropic state is stable when $\mu < 0$ and unstable when $\mu > 0$, while solving for $\mu = 0$ gives the transition. The sign of μ is set by two terms in Eq. (13). The first one is the average of the change of momentum in the forward direction ($\mathbf{p} \cdot \delta \mathbf{p}$) over the space of scattering parameters. As we will see, it can be of either sign, depending on the details of the interactions. Note that the average defined in Eq. (14) is conveniently normalized such that $\langle 1 \rangle_0 = 1$. In the second term of Eq. (13), the self-diffusion noise $D \geq 0$ acts on the scale of the free flight time $1/\lambda$ and has the effect of destroying polar order. For metric models, the interaction rate scales like $\lambda \propto \rho$. In this case, solving for $\mu = 0$ leads to the somewhat trivial linear dependance of the critical diffusion coefficient with density $D_c \propto \rho$ (or $\sigma_{0c} \propto \sqrt{\rho}$), as commonly reported in the literature.

In Eqs. (8) and (12), all the model-specific microscopic details of the interaction between particles appear only through the forward momentum change $\mathbf{p} \cdot \delta \mathbf{p}$. The latter

is positive when $\delta\mathbf{p}$ points forward, *i.e.* in the same “direction” as \mathbf{p} , see Fig. 1(right). It is often said that a scattering event “aligns” particles when it decreases the angular separation between the velocities, that is when $|\mathbf{p}'| > |\mathbf{p}|$. However, it is easy to see from Fig. 1, that this microscopic alignment property is a necessary condition for having $\mathbf{p} \cdot \delta\mathbf{p} > 0$, although not a sufficient one, since a large enough angular deviation of momentum can always bring \mathbf{p}' in the backward semi-plane. We learn here that $\mathbf{p} \cdot \delta\mathbf{p}$ is the proper quantity to evaluate the microscopic alignment taking place in a scattering event.

The mechanism of the instability of the isotropic state is clear: if there is some fluctuation of polar order $\psi \neq 0$, the momentum of two interacting particles is statistically more likely found along the direction of this fluctuation. Then, if $\langle \mathbf{p} \cdot \delta\mathbf{p} \rangle_0 > D/\lambda$, momentum is created on average along this same direction by binary scattering, building polar order faster than the self-diffusion noise is able to destroy.

2.4. Nature of the transition

To predict whether the transition is continuous or discontinuous, we go beyond linear order, expanding Eq. (8) up to order ψ^3 :

$$\frac{1}{\lambda} \frac{d\psi}{dt} = \mu\psi - \xi\psi^3, \quad (15)$$

where

$$\xi = \langle \left(\frac{1}{2} - \cos \Delta \right) \mathbf{p} \cdot \delta\mathbf{p} \rangle_0. \quad (16)$$

If $\xi > 0$ at the transition, the transition is continuous and the polar state $\psi \simeq \sqrt{\mu/\xi}$ emerges continuously as a new stable stationary state. If $\xi < 0$, the transition is discontinuous and one must expand Eq. (8) to higher orders in ψ to compute the new stable stationary state. The expression in Eq. (16) depends on the ansatz for the angular distribution. However, the sign is what matters for the prediction of the nature of the transition. One can show that a continuous transition is indeed predicted as such by Eq. (16), see Appendix A.

In Eq. (16), the factor $\frac{1}{2} - \cos \Delta$ gives a negative contribution for tangential scattering (low angles $|\Delta|$), and a positive contribution for frontal scattering (large angles $|\Delta|$). In models where tangential scattering dis-aligns while frontal scattering aligns, the transition is prone to be continuous. We will see below that models with interactions given by the Vicsek collision rule fall in this class of models. On the other hand, in models where tangential scattering mostly aligns and where frontal scattering mostly dis-aligns, coefficient ξ is more likely to be negative. There is thus the propensity for this kind of models to display a discontinuous transition rather than a continuous one. As we will see below, in a model of self-propelled hard disks with inelastic collisions, this qualitative argument gives a correct prediction.

2.5. Fluctuations of the order parameter

We can obtain informations on the fluctuations of the order parameter by computing the value of $\psi^2 = \mathbf{P}^2$ in the stationnary state. One way to do it is to start again from the momentum balance equation $N(\mathbf{P}' - \mathbf{P}) = \delta\mathbf{p}$. Taking the square, we obtain the balance equation

$$N(\mathbf{P}'^2 - \mathbf{P}^2) = 2\mathbf{P} \cdot \delta\mathbf{p} + \frac{1}{N}\delta\mathbf{p} \cdot \delta\mathbf{p}, \quad (17)$$

from which one can obtain a kinetic equation for \mathbf{P}^2 , using the same derivation than presented above. Finally, making use of the von Mises distribution ansatz, one can obtain a closed-form evolution equation. The derivation can be found in Appendix B. As it is not particularly instructive, we present here only the main result. In the isotropic state, the variance of \mathbf{P} is given by

$$\text{Var}[\mathbf{P}] = \langle \mathbf{P}^2 \rangle = \frac{1}{N} \frac{\frac{1}{2}\langle \delta\mathbf{p} \cdot \delta\mathbf{p} \rangle_0 + D/\lambda}{|\mu|}. \quad (18)$$

It scales like $1/N$ as expected. In the numerator, the fluctuations arise both from the fluctuations of $\delta\mathbf{p}$ in binary scattering events and from the fluctuations of the self-diffusion process. The denominator $|\mu|$ is the “restoring force”, which vanishes at the transition. The absolute value comes from μ being negative in the isotropic phase. In the isotropic phase, \mathbf{P} follows a gaussian distribution and it is easy to show that $\langle \psi \rangle^2 = \frac{\pi}{4}\langle \mathbf{P}^2 \rangle$, from which one obtains the variance of the scalar order parameter

$$\langle \psi^2 \rangle - \langle \psi \rangle^2 = (1 - \frac{\pi}{4})\langle \mathbf{P}^2 \rangle. \quad (19)$$

This prediction is in full agreement with numerical measurements in the three models studied below.

3. Application to models

We now come to the illustration of these mechanisms in the case of three different models. We also test numerically the accuracy of the von Mises ansatz. We focus the discussion on the binary scattering properties, illustrating the link between the alignment function $\int_{\zeta} \mathbf{p} \cdot \delta\mathbf{p}$ of the models and the corresponding collective behaviour. We thus study the models without any self-diffusion noise by setting $D = 0$. As we described quantitatively by Eq. (13), the $D > 0$ case shifts the transition by stabilizing the isotropic phase.

3.1. Mean-field binary Vicsek model

We first consider a non-metric model where interactions are binary, with a change of momentum that follows the collision rule of the Vicsek model. At every time-step, two randomly chosen particles among $N \gg 1$ collide, following the binary Vicsek collision rule: from pre-collision velocity angles θ_1 and θ_2 , the half-angle $\bar{\theta} = \text{Arg}(e^{i\theta_1} + e^{i\theta_2})$ is computed and randomly rotated to $\bar{\theta} + \eta_1$ and $\bar{\theta} + \eta_2$. The collisions noises η_1 and η_2 are two independent noises following a gaussian distribution of variance σ^2 ,

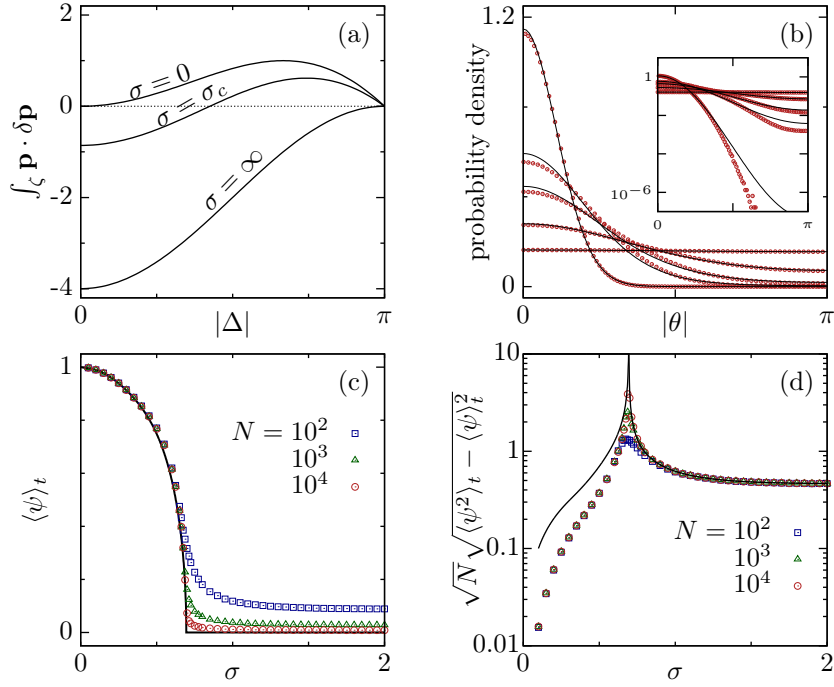


Figure 3. Mean-field binary Vicsek model. (a): The alignment function $\int_\zeta \mathbf{p} \cdot \delta \mathbf{p}$, for different values of the control parameter σ . (b): Angular distributions measured at $N = 10^4$ (symbols) and the corresponding ansatz distributions (lines). From top to bottom: $\sigma = 0.25, 0.5, 0.6, 0.675, 1$ (respectively $\psi \simeq 0.94, 0.77, 0.61, 0.32, 0.01$). Inset: the same but with vertical log-scale. (c), (d): Average in the steady state of the order parameter and its rescaled standard deviation. Symbols are numerical solution of the Boltzmann equation. Full black lines are theoretical predictions.

$P(\eta) = e^{-\eta^2/2\sigma^2}/\sqrt{2\pi\sigma^2}$. The two new angles are then assigned to the unit velocity vectors of the particles. The collision noise σ is used as the control parameter. As for the Vicsek model, it has the effect to blur out the alignment to the half-angle $\bar{\theta}$ and we expect an isotropic phase at large σ and a polar phase at small σ . An important difference with the Vicsek model, apart from the absence of space, is that interactions are only binary, whereas particles in the Vicsek model can interact through multiple interactions. The model is termed as a mean-field one, as a particle can interact with any other one, with no correlation of any kind. We mean that, by construction, the molecular chaos hypothesis holds exactly for this model, as the master equation that describes the dynamics is exactly the Boltzmann equation. Thus, the discrepancy between the theoretical predictions and the numerical data comes only from finite-size effects, which are neglectable here as we will see, and from the inaccuracy of the ansatz. This kind of mean-field models thus provides a way to test for the accuracy of the ansatz.

Let us first look at the theoretical predictions. It is easy to see that $\mathbf{p} \cdot \delta \mathbf{p} = |\mathbf{p}|(\cos \eta_1 + \cos \eta_2 - |\mathbf{p}|)$, where $|\mathbf{p}| = 2 \cos \frac{\Delta}{2}$. The integration over the collision noises

is performed using $\int d\zeta \equiv \int d\eta_1 d\eta_2 P(\eta_1)P(\eta_2)$. We obtain the alignment function

$$\int d\zeta \mathbf{p} \cdot \delta\mathbf{p} = 2 \cos \frac{\Delta}{2} \left(2e^{-\sigma^2/2} - 2 \cos \frac{\Delta}{2} \right). \quad (20)$$

This function of the incoming angular separation Δ , represented in Fig. 3(a), summarizes the microscopic dynamics averaged over the “internal” degrees of freedom of the scattering (here the collision noise): for $\sigma = 0$ it is always positive, all collisions align on average; for $\sigma = \infty$ it is always negative, there is no alignment on average. At intermediate σ , collision with a large, respectively small, incoming angle separation Δ align, respectively dis-align. Computing the coefficient μ now simply consists in averaging this function against the kinetic kernel K . Here, there is no spatial dependence of any kind, and K is just a constant. Using Eqs. (13) and (16), we integrate Eq. (20) over $\int d\Delta$, obtaining $\mu = \frac{8}{\pi}e^{-\sigma^2/2} - 2$ and $\xi = \frac{4}{3\pi}e^{-\sigma^2/2}$. Solving for $\mu = 0$, the transition occurs at $\sigma_c = \sqrt{2 \log(4/\pi)} \simeq 0.695$ and, because $\xi(\sigma_c) > 0$, the transition is continuous. To extend the predictions to the polar phase, we set $d\psi/dt = 0$ in Eq. (8) and solved it numerically, so to obtain the order parameter. These predictions are presented in Fig. 3 in full black lines.

We compare them to numerical results obtained using the following Monte-Carlo method [48]. Starting from N random angles $\theta_i(t)$, a pair of distinct particles (i, j) is chosen randomly, uniformly. The collision rule is then applied, obtaining the new angles $\theta_i(t+1)$ and $\theta_j(t+1)$. All other particles keep their angle. The procedure is repeated until the stationary state is reached. We then start to measure averages over time of quantities of interest. In our simulations, these averages typically involved 10^6 collisions, which gives us good enough statistics. Finite-size effects in the simulations are under control, as shown by the scaling in N in Fig. 3(d).

Quite remarkably the measured angles distributions compare well with the ansatz in the whole range of ψ , see Fig. 3(b). Time averages of the order parameter in the stationary state also compare very well with the theoretical prediction in the whole range of ψ , see Fig. 3(c). Concerning the fluctuations of the order parameter, one must distinguish the isotropic phase from the polar one. In the isotropic phase the predictions are excellent, see Fig. 3(d), confirming that the correlations are negligible. In the polar phase, the von Mises distribution ansatz is not supposed to be exact, which translates into a qualitative agreement only. Finally, increasing the size of the system, the divergence of the fluctuations at the transition is captured better and better.

3.2. Continuous-time hard disks Vicsek model

We next consider a metric model, with N hard disks of diameter $d_0 = 1$ moving in a periodic box of linear size L . The number density is $\rho = N/L^2$. In this model, speeds are fixed to $v_0 = 1$. As we do not consider self-diffusion, particles go in straight line until a collision occurs. Two particles interact when $|\mathbf{r}_1 - \mathbf{r}_2| = d_0$, their velocities are changed following the binary Vicsek collision rule, as already defined in the previous model (alignment to the half-angle and a collision noise with variance σ^2). A way to

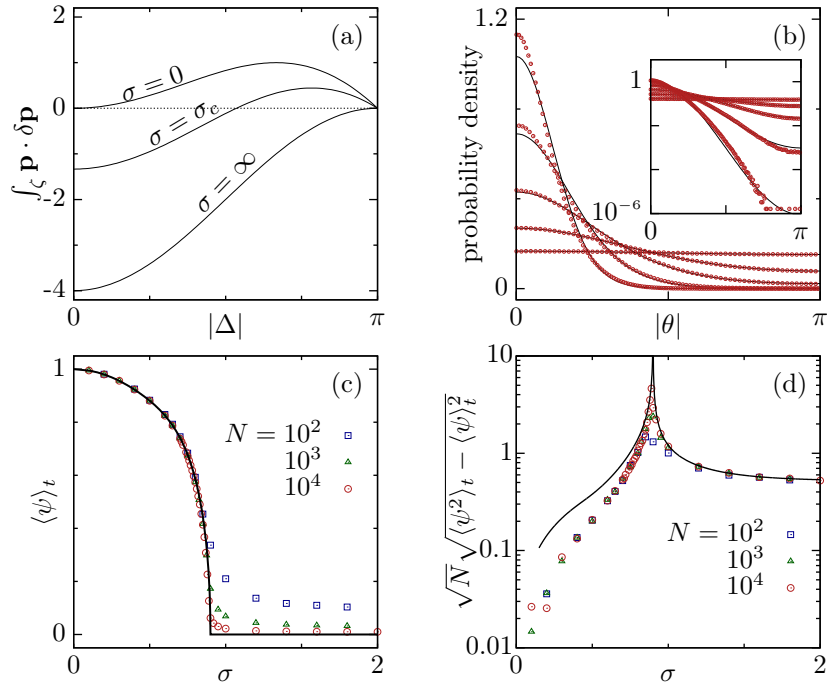


Figure 4. Continuous-time hard disks Vicsek model at density $\rho = 10^{-3}$. (a): The alignment function $\int_{\zeta} \mathbf{p} \cdot \delta \mathbf{p}$, for different values of the control parameter σ . (b): Angular distributions measured at $N = 10^4$ (symbols) and the corresponding ansatz distributions (lines). From top to bottom: $\sigma = 0.4, 0.6, 0.8, 0.88, 1$ (respectively $\psi \simeq 0.93, 0.83, 0.59, 0.30, 0.02$). Inset: the same but with vertical log-scale. (c), (d): Average in the steady state of the order parameter and its rescaled standard deviation. Symbols are numerical data from molecular dynamics simulations. Full black lines are theoretical predictions.

ensure that the interaction is always binary is to prevent particles to overlap. This is achieved by noticing that there is only one way to assign the two outgoing velocities to the two particles, out of the two possibilities. We choose to assign the velocities such that particles do not overlap, hence the terming of *hard* disks. Using this rule, the interaction between particles is binary and the interaction is made instantaneous, which has allowed to define a continuous-time model. The current model, in the dilute regime where molecular chaos hypothesis holds, is an actual implementation of the one studied theoretically in Refs. [12, 13], but not simulated therein. By comparison, in the original Vicsek model, the dynamics are discrete in time. As a consequence, particles behave like disks that can overlap at any time with one or many other particles. Note also that, in the Vicsek dynamics, a scattering event, even if binary, can last many time steps.

Here again, the collision noise σ is used as a control parameter. The collision rule being the same as for the mean-field Vicsek model, the alignment function $\int_{\zeta} \mathbf{p} \cdot \delta \mathbf{p}$ is *the same* as Eq. (20). For the theoretical description, the only difference stems in the kinetic kernel, which reads here $K(\Delta) \propto |\sin(\Delta/2)|$, as given by the construction of the Boltzmann cylinder. We also remind that the scattering rate is set by the density,

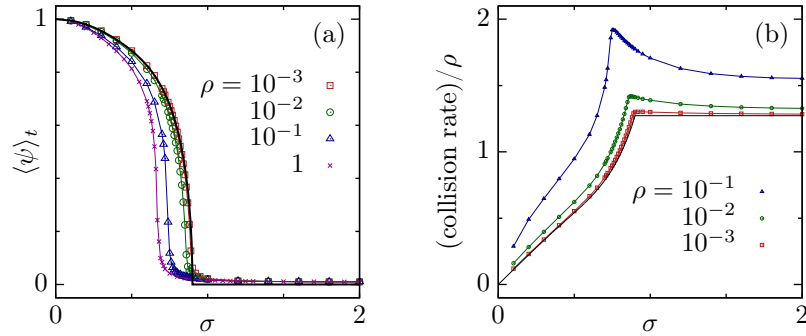


Figure 5. Continuous-time hard disks Vicsek model at densities $\rho = 10^{-3}, 10^{-2}, 10^{-1}$ and 1. (a): Polar order parameter. (b): Collision rate, rescaled. For clarity, the data at $\rho = 1$ is not plotted. At this density, the rescaled collision rate behaves qualitatively the same than for lower densities, but with much higher values (reaching around 28 as the maximal value at the transition). Symbols are numerical data, $N = 10^4$. Black lines are theoretical predictions at vanishing density.

$\lambda \propto \rho$. Again one can compute μ , following Eqs. (13), obtaining $\mu = \frac{8}{\pi} e^{-\sigma^2/2} - \frac{16}{3\pi}$, which cancels at $\sigma_c = \sqrt{2 \log(3/2)} \simeq 0.9005$. We recover the same results as in Refs. [12, 13]. We also find that the transition is continuous, $\xi(\sigma_c) > 0$. Remember that this statement only concerns the transition between homogeneous states. It does not rule out the discontinuous transition scenario reported for this system, which involves the destabilization of the homogeneous polar phase with respect to inhomogeneous solutions [12, 13]. Finally, we can also solve numerically Eq. (8) for the order parameter in the polar phase, see the black lines in Figs. 4 and Figs. 5(a).

We obtained numerical data in the stationary state of molecular dynamics simulations. In absence of noise, we used an event-driven method, which allowed us to probe more easily the low density regime. In order to prevent such large but finite wavelengths destabilization of the homogeneous state, we used small enough systems. No travelling bands were observed in our simulations, even at $N = 10^4$. As for the mean-field model studied above, the theoretical predictions are in very good agreement with the simulation data at low density $\rho = 10^{-3}$, see Fig. 4.

We also investigated finite density effects on the order parameter and the collision rate, as shown in Fig. 5. As density increases, deviations become more and more noticeable, although they are hardly seen at density below $\rho = 10^{-3}$. For the order parameter (Fig. 5(a)), an increase in density *stabilizes* the isotropic phase. This is in contrast with the most commonly reported effect of stabilization of the polar phase by density, in the presence of self-diffusion. In the present case, there is no self-diffusion ($D = 0$) and the transition shift comes from truly non-trivial correlations. For the collision rate, a quantity most easily measured in event-driven simulations, see Fig. 5(b), a prediction can be obtained by computing $\lambda\Phi_f^{\text{scat}}[1]$, using the von Mises distribution ansatz. The idea is simply to count +1 at each collision, instead of $\delta\mathbf{p}$ in kinetic equations such as Eq. (2). The result is plotted as a black full line in Fig. 5(b). In the

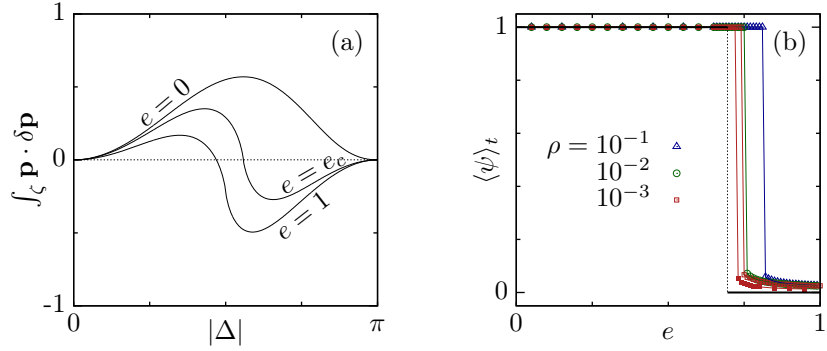


Figure 6. Self-propelled hard disks model with inelastic collisions, $\tau = 1$. (a): The alignment function $\int_C \mathbf{p} \cdot \delta \mathbf{p}$, for different values of the control parameter e . (b): Polar order parameter. Symbols: numerical data, $N = 1000$ (open symbols), $N = 4000$ (full symbols). Black lines are theoretical predictions at vanishing density.

isotropic phase, the collision rate is simply the constant $\lambda = 4\rho/\pi$. In the polar phase, it decreases smoothly as ψ is increased. This is again a pure kinetic effect. When polar order is higher, particles are more parallel, with smaller relative velocities, so it takes more time before a collision is likely to occur. The collision rate vanishes for $\psi = 1$, when all particles are strictly parallel. From the numerical data, we observe first that the overall collision rate is increased as density gets higher; second that, for a given density, the collision rate increases as the transition is approached from either side, reaching a finite maximal value at the transition. While the first feature is expected, as it happens also in equilibrium systems [20], the second one indicates a non-trivial dependance of the collision rate with density in the transitional regime. These effects cannot be understood on the basis of the Boltzmann formalism.

3.3. Inelastic self-propelled hard disks

Several works [30, 49, 50] have shown that pairwise dissipative interactions lead to global polarization in swarms of SPPs. In the present model, particles are hard disks of diameter $d_0 = 1$ that collide inelastically. The restitution coefficient $0 \leq e \leq 1$ of the inelastic collisions is used as a control parameter for the transition. Between collisions, the dynamics of particle i is given by

$$\frac{d\mathbf{r}_i}{dt} = \mathbf{v}_i, \quad (21)$$

$$\tau \frac{d\mathbf{v}_i}{dt} = \text{sign}(v_0 - |\mathbf{v}_i|) \hat{\mathbf{v}}_i, \quad (22)$$

where $\text{sign}(x)$ is -1, 0 or 1, respectively when x is negative, zero or positive. The r.h.s. term of Eq. (22) allows us to use event-driven methods to perform molecular dynamics simulations. It mimics the more standard exponential relaxation of the velocity \mathbf{v}_i to $\hat{\mathbf{v}}_i = \mathbf{v}_i/|\mathbf{v}_i|$ on a timescale τ .

For this model, the $\int_C \mathbf{p} \cdot \delta \mathbf{p}$ functions are computed numerically by simulating many binary scattering events at some fixed incoming angular separation Δ , varying

the impact parameter b uniformly, see Fig. 6(a). From these data, we compute μ and ξ , using Eqs. (13) and (16). We find a transition at $e_c \simeq 0.70$. Because $\xi(e_c) < 0$, the transition is predicted to be discontinuous. The results are in full agreement with direct molecular dynamics simulations with a random isotropic state as initial conditions. As shown in Fig. 6(b), the transition is indeed highly discontinuous.

Around the transition $e = e_c$, as seen in Fig. 6(a), tangential collisions (low $|\Delta|$) align, while frontal collisions (high $|\Delta|$) dis-align. This is in total contrast with the binary Vicsek collision rule, see Fig. 3(a) or Fig. 4(a). Note that tangential collisions align for all values of e . As a consequence, the fully polar state $\psi = 1$ is stable for all values of e . Indeed, when $\psi \simeq 1$, particles are all quite parallel, so that binary scattering only occurs at low $|\Delta|$. In this scattering regime, $\mathbf{p} \cdot \delta\mathbf{p} > 0$, so that polar order increases back to $\psi = 1$. There is thus a coexistence of stability between the $\psi = 1$ and $\psi = 0$ states, hence a discontinuous transition. Here, as opposed to the previous model, higher densities tend to stabilize the polar phase, also in absence of self-diffusion.

4. Conclusion

In summary, proposing an ansatz for the velocity angular distribution, we have derived an equation for the evolution of the momentum of systems of polar active particles with fixed speed. The weakly non-linear analysis around the isotropic state is given by Eqs. (12) and provides an intuitive way of anticipating the transition to collective motion in systems of polar active particles: the existence and the nature of the transition are essentially governed by the way $\int_\zeta \mathbf{p} \cdot \delta\mathbf{p}$ depends on the incoming angle. As an important consequence, the forward component of momentum change, $\mathbf{p} \cdot \delta\mathbf{p}$, is the proper quantity to characterize the alignment of binary scattering. Also, we tested the fully non-linear equation on three different kinds of models, and showed that the von Mises ansatz describes quite well the velocity angular distribution, even for large polarization. This shows that knowing the value of the order parameter, alone, already gives much qualitative information about the kinetics. Of course, predictions of more subtle effects in the polar phase should require better approximation schemes. These encouraging results naturally call for the extension of our analysis to models in which the particle speeds are free to fluctuate. Our work may also be adapted to describe the transition towards nematic states or three dimensional systems.

Acknowledgements

The authors would like to thank E. Bertin for enlightening discussions.

Appendix A. On the sign of the cubic term

As the derivation of Eq. (16) involves the use of an ansatz, it is not “exact” and one should worry about the sign of ξ being wrong. Let us now compare the expression

of Eq. (16) with the one obtained in references [17], where the starting point is also the Boltzmann equation, but where the hydrodynamics equations are derived using a different closure scheme. We first briefly describe how these equations are obtained. Starting from the Fourier series $f(\theta, t) = \frac{1}{2\pi} \sum_k f_k(t) e^{-ik\theta}$, the Boltzmann equation can be written in Fourier space. The result is an infinite number of coupled equations: the time evolution of the k -th mode is given as a function of the other modes. Next, the following scaling hypothesis is assumed close to the transition [17]: $|f_k| \sim \epsilon^{|k|}$ and $\partial_t \sim \epsilon$, for some small parameter ϵ . Neglecting all contributions of order ϵ^4 and those of higher order, the Boltzmann equation reduces to [17]:

$$\partial_t f_0 = 0, \quad (\text{A.1})$$

$$\partial_t f_1 = \mu_1 f_1 - \xi_1 f_1^* f_2, \quad (\text{A.2})$$

$$\partial_t f_2 = \mu_2 f_2 + \gamma f_1^2, \quad (\text{A.3})$$

The first equation states that a homogeneous density field stays homogeneous. The second one is the analog of our evolution equation for the vectorial order parameter \mathbf{P} . The third equations describe the evolution of the nematic order parameter. We have discarded the equation for $\partial_t f_3$ because f_1 and f_2 do not depend on f_3 . As long as the scaling hypothesis holds uniformly, these equations can be considered as “exact”. Note that they apply only in the case $\xi_1 > 0$, since $\xi_1 < 0$ would require to include higher order terms.

In what follows, we suppose that the isotropic state is linearly stable with respect to the nematic phase, hence $\mu_2 < 0$, and consider the slightly polar state, $\mu_1 > 0$ with $\mu_1 \simeq 0$. As $|f_1| \neq 0$, we are free to choose the reference direction by setting $f_1^* = f_1 > 0$. In the stationnary state, Eqs. (A.2) and (A.3) are equated to zero, so to obtain

$$|f_1|^2 = \frac{\mu_1}{\xi_1} \frac{|\mu_2|}{\gamma}, \quad f_2 = \frac{\gamma}{|\mu_2|} f_1^2. \quad (\text{A.4})$$

We see from the first equation that one must have $\gamma > 0$ and from the second that $f_2 > 0$. The expression of the stationnary f_2 in Eq. (A.4) can be used in Eq. (A.2), which then reads

$$\partial_t f_1 = \mu_1 f_1 - \xi_1 \frac{\gamma}{|\mu_2|} f_1^* f_1^2. \quad (\text{A.5})$$

We see that the “exact” cubic coefficient is given by $\xi_1 \gamma / |\mu_2| > 0$. Note that it has the same sign as $\xi_1 > 0$.

We now come back to our results, obtained from the von Mises distribution ansatz. The expansion in powers of f_1 of the ansatz in Eq. (7) reads

$$f_\psi(\theta) = \frac{1}{2\pi} + \frac{1}{\pi} (\psi \cos \theta + \psi^2 \cos 2\theta + \dots). \quad (\text{A.6})$$

One important difference here is that the second Fourier mode is slaved to the first one, such that $f_2 = f_1^2$, instead of having Eq. (A.4). Thus, one finds $\partial_t f_1 = \mu_1 f_1 - \xi_1 f_1^3$, instead of Eq. (A.5). By identifying this equation with Eq. (15), it is shown that (i) $\mu_1 = \mu$, as given by Eq. (13), (ii) $\xi_1 = \xi$, as given by Eq. (16), (iii) the cubic term in Eq. (15) has the correct sign. Thus, if the transition predicted by Eq. (A.5)

is continuous, Eq. (15) also predicts a continuous transition: both approaches are consistent. Interestingly, this mainly comes from f_2 and f_1 sharing the same sign for a continuous transition, which means that both the polar mode and the nematic modes are in phase, a property also possessed by the von Mises distribution.

When $\xi_1 < 0$, one has to consider higher order “exact” equations. Unfortunately, even the order 7 equations are not well behaved [17].

Appendix B. Fluctuations of the order parameter

Here, we derive an expression for the variance of the order parameter. We start from Eq. (17), the balance equation for the momentum:

$$N(\mathbf{P}'^2 - \mathbf{P}^2) = 2\mathbf{P} \cdot \delta\mathbf{p} + \frac{1}{N} \delta\mathbf{p} \cdot \delta\mathbf{p}. \quad (\text{B.1})$$

Assuming that the system is non chiral, we can follow the procedure already used for deriving Eq. (2). We find

$$\frac{1}{\lambda} \frac{d\mathbf{P}^2}{dt} = 2\psi \Phi_f^{\text{scat}} [\hat{\mathbf{p}} \cdot \delta\mathbf{p} \cos \bar{\theta}] + \frac{2}{N} \Phi_f^{\text{scat}} [\delta\mathbf{p} \cdot \delta\mathbf{p}] - 2\frac{D}{\lambda} \left(\psi^2 - \frac{1}{N} \right), \quad (\text{B.2})$$

with Φ_f^{scat} defined in Eq. (3). Note that this equality stands at the level of ensemble average. Using the von Mises distribution ansatz, the integration over $\bar{\theta}$ can be performed explicitly and this expression becomes

$$\frac{1}{\lambda} \frac{d\mathbf{P}^2}{dt} = 2\psi F(\psi) + \frac{2}{N} G(\psi) - 2\frac{D}{\lambda} \left(\psi^2 - \frac{1}{N} \right), \quad (\text{B.3})$$

where $F(\psi)$ is already given by Eq. (9) and where

$$G(\psi) = \int_{-\pi}^{\pi} \frac{d\Delta}{2\pi} \int d\zeta K(\Delta, \zeta) \frac{I_0(2\kappa(\psi) \cos \frac{\Delta}{2})}{I_0^2(\kappa(\psi))} \frac{1}{2} \delta\mathbf{p} \cdot \delta\mathbf{p}(\Delta, \zeta). \quad (\text{B.4})$$

Now, consider the ensemble averaged stationnary state \mathbf{P}_* , and the trajectory of the system around this average: $\mathbf{P}(t) = \mathbf{P}_* + \delta\mathbf{P}(t)$, with $\delta\mathbf{P}(t)$ assumed to be of order $1/\sqrt{N}$. The order 0 of Eq. (B.3) gives the condition for the stationnary state, $F(\psi_*) - (D/\lambda)\psi_* = 0$, while orders $1/\sqrt{N}$ and $1/N$ are respectively

$$\frac{1}{\lambda} \frac{d\mathbf{P}_* \cdot \delta\mathbf{P}}{dt} = \left(F'(\psi_*) - \frac{D}{\lambda} \right) \mathbf{P}_* \cdot \delta\mathbf{P}, \quad (\text{B.5})$$

$$\frac{1}{2\lambda} \frac{d(\delta\mathbf{P})^2}{dt} = \left(F'(\psi_*) - \frac{D}{\lambda} \right) (\delta\mathbf{P})^2 + \frac{1}{N} \left(G(\psi_*) + \frac{D}{\lambda} \right), \quad (\text{B.6})$$

where $F'(\psi) \equiv dF/d\psi$. The first equation is the stability condition of the stationnary state, thus requiring that $F'(\psi_*) < \frac{D}{\lambda}$. Equating the second equation to zero, we get the variance of the order parameter in the stationnary state:

$$\text{Var}[\mathbf{P}] = (\delta\mathbf{P})^2 = -\frac{1}{N} \frac{G(\psi) + D/\lambda}{F'(\psi_*) - D/\lambda}. \quad (\text{B.7})$$

The minus sign comes from the denominator being negative. Note that this expression is not expected to be accurate quantitatively in the polar phase. In the isotropic state, this expression becomes Eq. (18).

References

- [1] Ramaswamy S 2010 *Annu Rev Conden Ma P* **1** 323–345
- [2] Marchetti M C, Joanny J F, Ramaswamy S, Liverpool T B, Prost J, Rao M and Simha R A 2013 *Rev. Mod. Phys.* **85** 1143–1189
- [3] Vicsek T, Czirók A, Ben-Jacob E, Cohen I and Shochet O 1995 *Phys. Rev. Lett.* **75** 1226–1229
- [4] Czirók A, Stanley H E and Vicsek T 1997 *Journal of Physics A: Mathematical and General* **30** 1375
- [5] Grégoire G and Chaté H 2004 *Phys. Rev. Lett.* **92** –
- [6] Chaté H, Ginelli F, Grégoire G and Raynaud F 2008 *Phys. Rev. E* **77** –
- [7] Ginelli F and Chaté H 2010 *Phys. Rev. Lett.* **105** 168103
- [8] Vicsek T and Zafeiris A 2012 *Physics Reports* **517** 71–140
- [9] Toner J, Tu Y and Ramaswamy S 2005 *Annals of Physics* **318** 170–244
- [10] Toner J and Tu Y 1995 *Phys. Rev. Lett.* **75** 4326–4329
- [11] Toner J and Tu Y 1998 *Phys. Rev. E* **58** 4828–4858
- [12] Bertin E, Droz M and Grégoire G 2006 *Phys. Rev. E* **74** 22101
- [13] Bertin E, Droz M and Grégoire G 2009 *Journal of Physics A Mathematical General* **42** 445001
- [14] Ihle T 2011 *Phys. Rev. E* **83** 030901
- [15] Chou Y L, Wolfe R and Ihle T 2012 *Phys. Rev. E* **86** 021120
- [16] Peshkov A, Ngo S, Bertin E, Chaté H and Ginelli F 2012 *Phys. Rev. Lett.* **109** 098101
- [17] Peshkov A, Bertin E, Ginelli F and Chaté H 2014 *Eur. Phys. J. Special Topics* **223** 1315–1344
- [18] Ihle T 2014 *Eur. Phys. J. Special Topics* **223** 1293–1314
- [19] Caussin J B, Solon A, Peshkov A, Chaté H, Dauxois T, Tailleur J, Vitelli V and Bartolo D 2014 *Phys. Rev. Lett.* **112** 148102
- [20] Hansen J P and McDonald I R 1976 *Theory of simple liquids* (London: Academic Press)
- [21] Kudrolli A, Lumay G, Volfson D and Tsimring L S 2008 *Phys. Rev. Lett.* **100**
- [22] Deseigne J, Dauchot O and Chaté H 2010 *Phys. Rev. Lett.* **105**
- [23] Palacci J, Cottin-Bizonne C, Ybert C and Bocquet L 2010 *Phys. Rev. Lett.* **105** –
- [24] Theurkauff I, Cottin-Bizonne C, Palacci J, Ybert C and Bocquet L 2012 *Phys. Rev. Lett.* **108** 268303
- [25] Deseigne J, Léonard S, Dauchot O and Chaté H 2012 *Soft Matter* **8** 5629
- [26] Bricard A, Caussin J B, Desreumaux N, Dauchot O and Bartolo D 2013 *Nature* **503** 95–98
- [27] Palacci J, Sacanna S, Steinberg A P, Pine D J and Chaikin P 2013 *Science* **339** 936–940
- [28] Kumar N, Soni H, Ramaswamy S and Sood A K 2014 *Nat. Comm.* **5** 4688
- [29] Peruani F, Deutsch A and Bär M 2006 *Phys. Rev. E* **74** 30904
- [30] Grossman D, Aranson I S and Ben-Jacob E 2008 *New Journal of Physics* **10** 023036
- [31] Henkes S, Fily Y and Marchetti M C 2011 *Phys. Rev. E* **84** –
- [32] Fily Y and Marchetti M C 2012 *Phys. Rev. Lett.* **108**(23) 235702
- [33] Redner G S, Hagan M F and Baskaran A 2013 *Phys. Rev. Lett.* **110** 055701
- [34] Weber C A, Hanke T, Deseigne J, Léonard S, Dauchot O, Frey E and Chaté H 2013 *Phys. Rev. Lett.* **110** 208001
- [35] Solon A P and Tailleur J 2013 *Phys. Rev. Lett.* **111**(7) 078101
- [36] Solon A P, Chaté H and Tailleur J 2015 *Phys. Rev. Lett.* **114**(6) 068101
- [37] Romensky M, Lobaskin V and Ihle T 2014 *Phys. Rev. E* **90**(6) 063315
- [38] Ballerini M, Cabibbo N, Candelier R, Cavagna A, Cisbani E, Giardina I, Lecomte V, Orlandi A, Parisi G, Procaccini A and others 2008 *Proceedings of the National Academy of Sciences* **105** 1232
- [39] Degond P, Appert-Rolland C, Pettré J and Theraulaz G 2013 *Kinetic and Related Models* **6**(4) 809–839
- [40] Albi G, Balagué D, Carrillo J A and von Brecht J 2014 *SIAM J. Appl. Math.* **74** 794–818
- [41] Deseigne J, Léonard S, Dauchot O and Chaté H 2012 *Soft Matter* **8** 5629–5639

- [42] Bricard A, Caussin J B, Desreumaux N, Dauchot O and Bartolo D 2013 *Nature* **503** 95–98
- [43] Hanke T, Weber C A and Frey E 2013 *Phys. Rev. E* **88**(5) 052309
- [44] Kardar M 2007 *Statistical Physics of Particles* (Cambridge)
- [45] Watson G 1982 *Journal of Applied Probability* **19** 265–280
- [46] Degond P, Frouvelle A and Liu J G 2013 *J. Nonlinear Sci.* **23** 427–456
- [47] Chepizhko O and Kulinskii V 2014 *Physica A* **415** 493–502
- [48] Bird G A 1970 *Physics of Fluids (1958–1988)* **13** 2676–2681
- [49] Lobaskin V and Romenskyy M 2013 *Phys. Rev. E* **87**(5) 052135
- [50] Coburn L, Cerone L, Torney C, Couzin I D and Neufeld Z 2013 *Physical Biology* **10** 046002